Bull Vo' ;anol (1991) 53:579-596

Bulletin of
Volcanology

© Springer-Verlag 1991

The roles of magma and groundwater in the phreatic eruptions at Inyo Craters, Long Valley Caldera, California

Larry G Mastin*

Department of Applied Earth Sciences, Stanford University, USA

Received March 1990, Accepted February 19, 1991

Abstract. The Inyo Craters (North Inyo Crater and South Inyo Crater), and a third crater, Summit Crater, are the largest of more than a dozen 650- to 550-yr-B.P. phreatic craters that lie in a 1-km-square area at the south end of the Inyo Volcanic Chain, on the west side of the Long Valley Caldera in eastern California. The three craters are aligned within a 1-km-long north-south system of fissures and normal faults, and coincide in age with aligned magmatic vents farther north in the Inyo Volcanic Chain, suggesting that they were all produced by intrusion of one or more dikes. To study the sequence and mechanisms of the eruptions, the deposits were mapped, sampled, and compared with subsurface stratigraphy obtained from the core of a slant hole drilled directly below the center of South Inyo Crater from the southwest. The deposits from the two Inyo Craters are fine-grained (median diameter less than 1 mm), are several meters thick at the crater walls, and cover at most a few km^2 of ground surface. Stratigraphic relationships between the Inyo Craters and Summit Crater indicate that the eruptions proceeded from north to south, overlapped slightly in time, and produced indistinctly plane-parallel bedded, poorly sorted deposits, containing debris derived primarily from within 450 m of the surface. Debris from the deepest identifiable unit (whose top is at 450 m depth) is present at the very base of both Inyo Craters deposits, suggesting that the eruptive vents were open and tapping debris from at least that depth, probably along preexisting fractures, even at their inception. According to ballistic studies, the greatest velocity of ejected blocks was of the order of 100 m/s. All eruptions, particularly the least powerful, selectively removed debris from the finest-grained, most easily eroded subsurface units. Although juvenile fragments have been previously identified in these deposits, they are confined primarily to the grain-size fraction smaller than 0.25 mm dia. and probably did not constitute more than several percent of the deposit. It is therefore suggested that these juvenile fragments were not the main source of heat for the eruptions, and that the eruptions were caused either by: (1) heating of water by fragmented magma that was not ejected before the eruption shut off; (2) slow heating (over months to years) of groundwater under confined conditions without fragmentation of magma, followed by a second process (pressure buildup, seismic faulting, or intrusions) that breached the confinement; or (3) breach of a pre-existing confined geothermal aquifer.

Introduction

In the past 20 years, our understanding of the mechanisms of explosive, pyroclastic eruptions and the nature of their deposits has advanced considerably. Careful examination of pyroclastic deposits (e.g. Walker 1971), theoretical modelling of eruptive dynamics (e.g. Wilson and Head 1981), and certain key observations (e.g. Moore et al. 1966) have helped to determine what factors are responsible for the explosivity of eruptions and for the processes that produce observed depositional features. Among other things, investigators have developed a greater appreciation for the importance of external (i.e. non-magmatic) water in controlling the explosivity of eruptions. Eyewitness accounts have documented an increase in explosivity when magma contacts water (Williams and McBirney 1979, p. 249). Experimental studies (e.g. Wohletz and McQueen 1984) suggest an optimal ratio of magma to groundwater which results in maximum explosive power. In recent years, the explosiveness of eruptions has been attributed with increasing frequency to magma-groundwater mixing (e.g. Fisher and Schmincke 1984, p. 231).

Recent discussions of phreatomagmatic eruptions have considered them in the context of a spectrum of eruptive types which ranges from purely phreatic to purely magmatic (Wohletz and McQueen 1984). Within this spectrum, the most puzzling, least studied, and

* now at U.S. Geological Survey, Cascades Volcano Observatory, 5400 MacArthur Blvd, Vancouver, WA 98661, USA

most poorly understood are those at the phreatic end: those whose deposits contain little or no juvenile debris. Compared with magmatic and phreatomagmatic eruptions or deposits, of which dozens to hundreds have been studied in detail, only a handful of phreatic eruptions or deposits have been carefully investigated. Many such eruptions occur in hydrothermal areas without any clear associated magmatic activity (e.g. White 1955; Muffler et al. 1971; Nelson and Giles 1985; Hedenquist and Henley 1985). Others were closely associated with volcanism (Finch 1943; Lloyd 1959; Prinz 1970; Nairn 1979; Nairn and Wiradiradja 1980; Christiansen and Peterson 1981) or occurred in volcanic craters accompanied by seismic tremor suggestive of subsurface magma flow (Nairn et al. 1979; Shepherd and Sigurdsson 1982; Feuillard et al. 1983).

Thus there is considerable uncertainty regarding the relative importance of magma as opposed to geothermal water in providing the heat that produced many of these eruptions. Evidence which can be used to separate these two processes requires both information from the deposits and the rare availability of subsurface data. The most useful information, in the form of drill core, has generally not been available. During the 1980s this need has been addressed by a Department of Energy, Office of Basic Energy Sciences-funded project which included the drilling of four boreholes into flows or feeder vents of a set of 550–650 yr. B.P., silicic volcanoes in the Inyo Volcanic Chain on the west side of the Long Valley Caldera in eastern California. The most recent of these holes was drilled beneath a 200-m-diameter phreatic crater, South Inyo Crater, at the south end of the Inyo Chain. The subsurface stratigraphy below Inyo Craters, and many of the characteristics of the eruptive vent as inferred from the drill core, have already been reported by Eichelberger et al. (1988). This paper reports on a study of the surface deposits from the Inyo Craters' eruptions, and their relationship to the structure and stratigraphy in the subsurface.

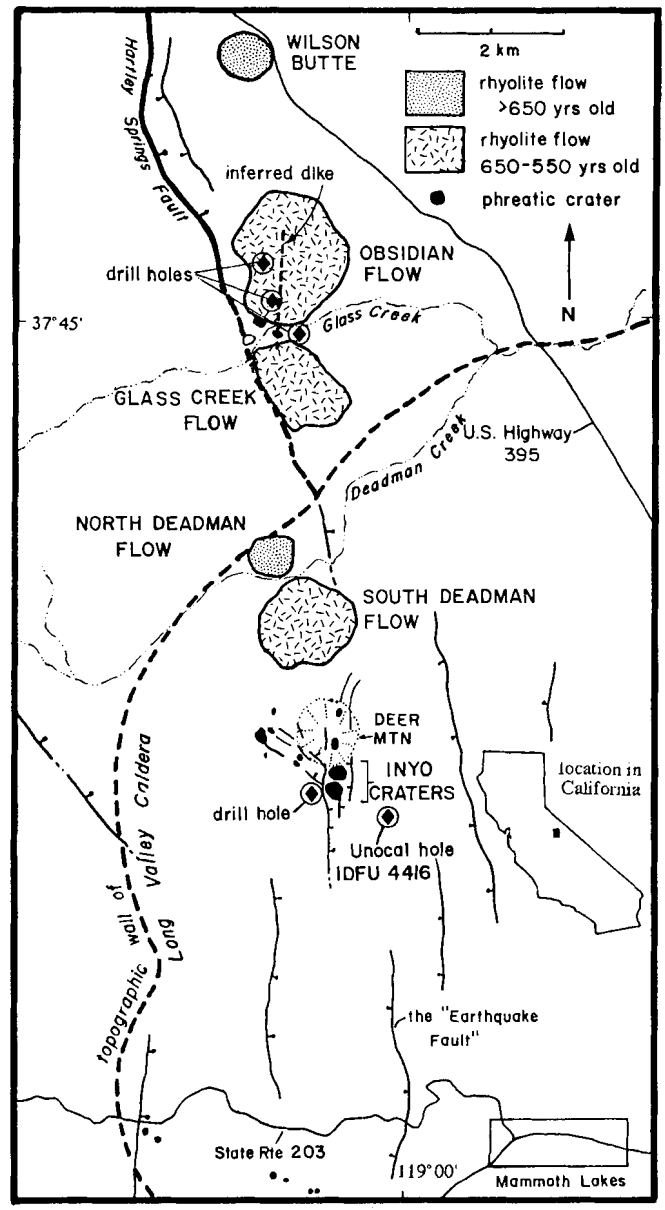

Fig. 1. Map of the Inyo volcanic chain

Geologic setting

The Inyo Craters (North Inyo Crater and South Inyo Crater) are the largest of about a dozen phreatic eruptive vents that lie at the south end of the Inyo Volcanic Chain, on the west side of the Long Valley Caldera in eastern California (Fig. 1). Silicic volcanismin this region began about 2.1 Ma (Metz and Mahood 1985) and climaxed 0.73 Ma during the eruption of the Bishop Tuff and collapse of the Long Valley Caldera (Bailey et al. 1976). Volcanic activity since the formation of the caldera has included eruptions of aphyric "early rhyolite" in and around the resurgent dome in the center of the caldera, hornblende-biotite "moat rhyolite" around the periphery of the resurgent dome, rhyodacite in the west moat of the caldera, and trachybasalts and trachyandesites in and around the west moat.

Holocene volcanism within the caldera has been confined entirely to the Inyo Volcanic Chain (Fig. 1). The most recent magmatic eruptions in the Inyo chain (Miller 1985) came nearly simultaneously from the vents of Obsidian Flow, Glass Creek Flow, and South Deadman Flow. The growth of these rubbly, steep-sided rhyolitic lava flows, up to 1.7 km in diameter and 50 to 100 m high, was preceded by large pyroclastic eruptions from the same vents. These eruptions were accompanied or followed a short time later by several phreatic eruptions from Glass Creek in the north (Miller 1985) to Mammoth Mountain in the south (Huber and Rinehart 1965; Miller 1985). The similarity in age of the eruptions, their alignment with faults and fissures along a single north-south trend, geochemical data, and drill-hole data indicate that they were fed by one or more north-south-trending dike segments (Bailey et al. 1983; Pollard et al. 1984; Miller 1985; Sampson and Cameron 1987; Mastin and Pollard 1988). Surface deformation features around the Inyo Craters

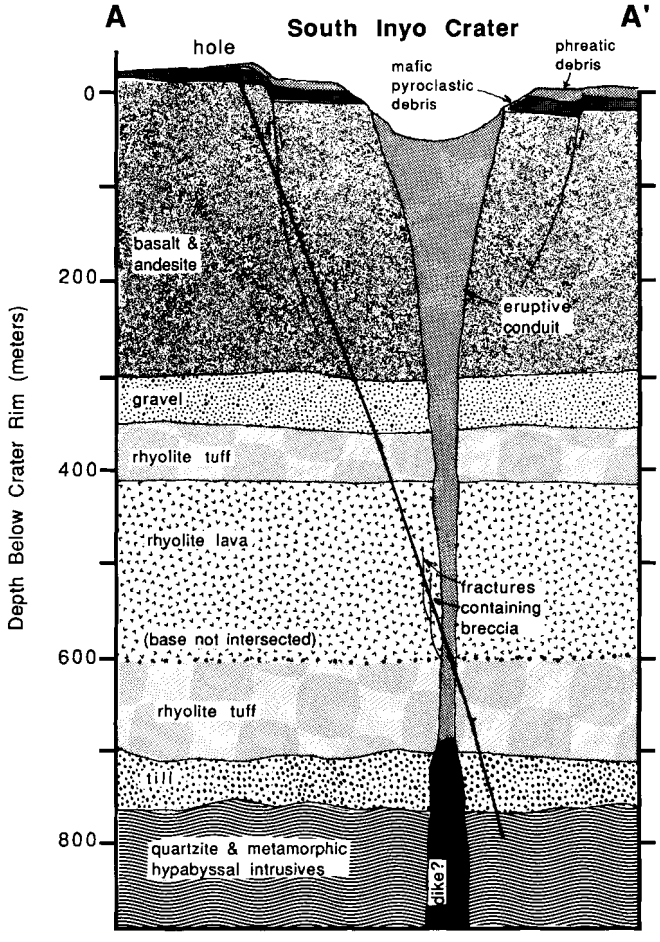

Fig. 2. Cross section of stratigraphy beneath South Inyo Crater. Location of cross section given by line A–A′ in Fig. 3

(Mastin and Pollard 1988) suggest that a large dike lies several hundred meters to perhaps more than a kilometer below the surface.

The deposits from the Inyo Craters and nearby phreatic eruptions all overlie and therefore are younger than the pyroclastic deposits from the South Deadman and Glass Creek vents. At South Inyo Crater radiocarbon dates and tree-ring studies of uncharred wood in the phreatic debris (Wood 1977) indicate that it erupted about 550±60 yr. ago, at about the same time as the magmatic eruptions.

The stratigraphy below the Inyo Craters is well constrained from two boreholes: the previously mentioned core hole directly beneath the crater ("Inyo 4"), and a 1799-m-deep vertical hole drilled by Unocal Geothermal Divison (Suemnicht 1987; Suemnicht and Varga 1988) 700 m southeast of South Inyo Crater (Fig. 1). The core from Inyo 4 (Fig. 2) shows that the stratigraphy in the uppermost 305 m below the South Inyo Crater rim consists of massive basaltic lava flows and pyroclastic deposits. The hand sample and thin section petrology of this unit does not change consistently with depth, but chemically the unit grades downward from trachyandesite to trachybasalt (referred to for brevity as andesite and basalt) (T. A. Vogel, Mich. St. Univ., written communication, 1988). Undifferentiated debris from this unit is referred to as "basalt" or "basaltic". Lithologic units below the basalt include (with increasing depth) multi-lithic gravel bearing rounded clasts up to 15 cm in diameter; early rhyolite tuff; an early rhyolite flow; early rhyolite tuff; a multi-lithic deposit (perhaps the Sherwin till) containing clasts up to 2 m in diameter; and brecciated quartzite basement below 762 m depth with hypabyssal intrusives (Eichelberger et al. 1988). Directly beneath the crater, three breccia zones (discussed in detail below) were encountered in the drill core. They were inferred to be parts of the eruptive conduit because they contain clasts from higher stratigraphic units (Eichelberger et al. 1988).

The information from Unocal hole IDFU 44-16 suggests considerable spatial variability in stratigraphy in this area. In the Unocal hole, the basement is 900 m lower than in Inyo 4 and is overlain by approximately 400 m of Tertiary andesites and dacites, and 250 m of Bishop Tuff, both of which are absent in Inyo 4. These differences suggest either: (1) that a major east-side-down normal fault lies between these two wells and that the Bishop Tuff and Tertiary volcanic rocks were either not deposited or were eroded away on the west; or (2) that the quartzite below South Inyo Crater is part of a slump block that covers deeper-lying Bishop Tuff and Tertiary volcanic units not penetrated by Inyo 4.

There is currently no surface evidence of a hydrothermal system in the Inyo Craters area, and there is no significant amount of hydrothermal alteration of rocks retrieved from the Inyo 4 drill core. However abundant well data (e.g. Sorey 1985; Suemnicht and Varga 1988; Sorey et al. 1991) indicate that the west side of the Long Valley Caldera has been the main source of heat for the caldera's currently active geothermal system. The main source is currently thought to be several kilometers east of South Inyo Crater. Although the Inyo 4 drillhole recorded a maximum temperature of only 83° C at 400 m depth (Eichelberger et al. 1988), the maximum temperature in Unocal hole IDFU 44-16 reached 218° C near the top of the Bishof Tuff at 1080 m depth (Suemnicht and Varga 1988).

The craters

The Inyo Craters and associated phreatic eruptive centers (Fig. 3) form three distinct clusters that lie on two structural trends. Two clusters (the two westernmost shaded areas in Fig. 3) lie at the center and the northwest end respectively, of a 1-km-long, northwest-trending set of scarps and linear depressions that are inferred from their topography to be faults and fissures. This trend of fissures may represent older structures, as they coincide in orientation with older major faults in the Sierra Nevada basement that intersect the northwest side of the caldera (Bailey 1989). However fracture patterns in the Inyo chain mapped by Fink (1985) and Mastin and Pollard (1988) suggest that this area may lie between two NNE-trending en echelon Inyo dike segments (one beneath the Inyo Craters and one beneath

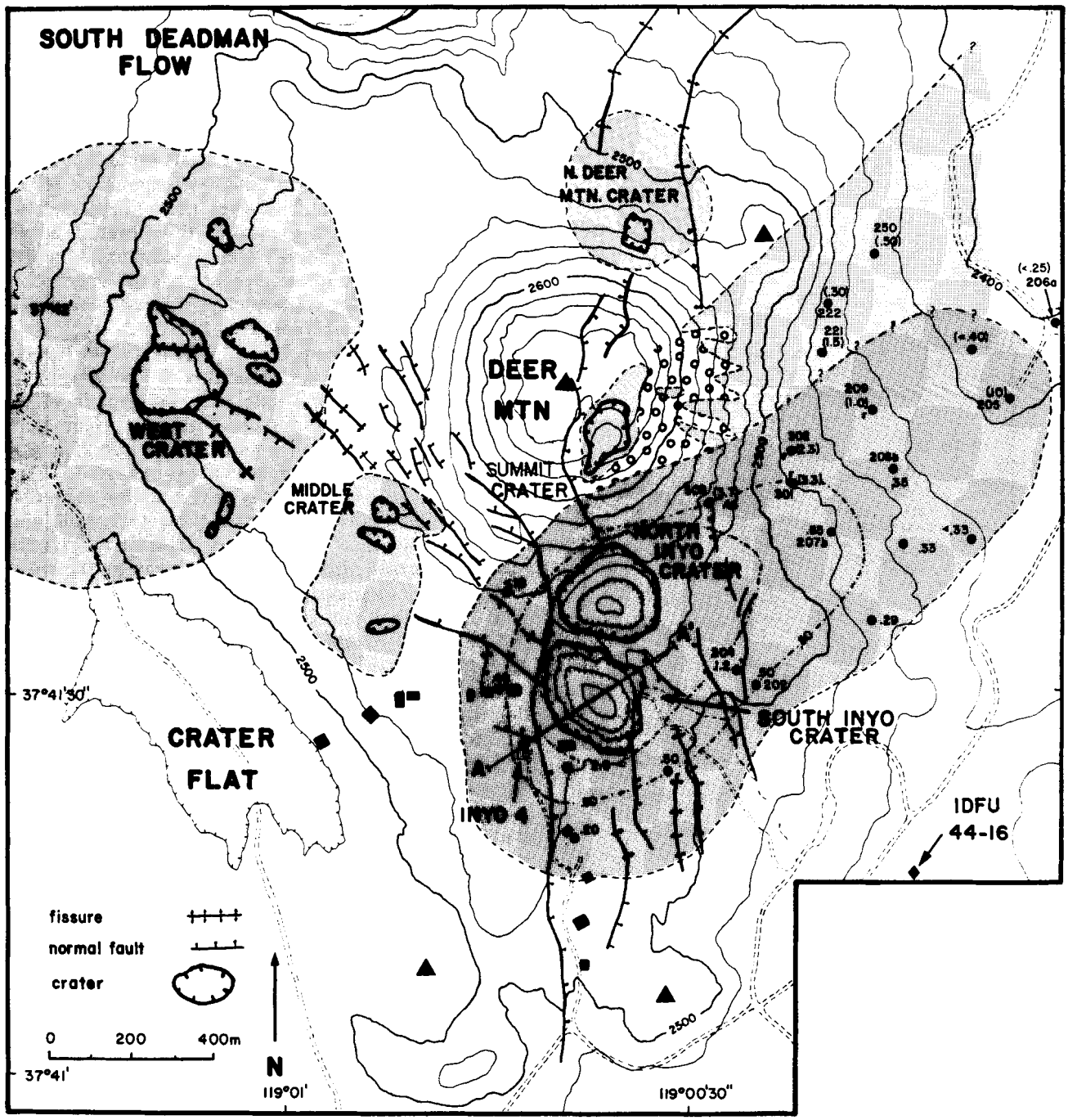

Fig. 3. Map of the Inyo Craters area showing the extent of eruptive-deposits. *Light shading* indicates the extent of eruptive debris from all craters. *Daker shading* indicates the extent of eruptive debris from South Inyo Crater. *Circle-dot pattern* on the east side of Deer Mountain indicates region where phreatic debris is patchy due to slumping. *Dot-dashed lines* are approximate isopachs for the deposits from South Inyo Crater. Locations of shovel pits and outcrops of debris are shown by *solid black dots*. Thickness values (in meters) of undifferentiated phreatic debris are enclosed in parentheses. Thickness values of South Inyo Crater deposit, where identified, are not in parentheses. *"r"* indicates reworked deposits. *Black rectangles* south and west of South Inyo Crater indicate locations of staked-out areas where block tallies were obtained for lithologic and ballistic analysis. *Black triangles* indicate locations of pre-Inyo vents. Elevation contours are in meters. The craters labeled West Crater, Middle Crater, Summit Crater, and North Deer Mountain Crater, were previously unnamed but were given these names in this paper for the purpose of identification

West Crater, Fig. 3) and that fractures could have been created or enlarged by a stress concentration between the dike segments.

The vents in the westernmost clusters of craters are generally smaller and less distinct than those in the eastern cluster. The lowest level of eruptive activity apparently occurred by expulsion of small amounts of debris (accidental fragments from underlying units) out of open fissures. Around intermediate-sized eruptive vents (e.g. Middle Crater, Fig. 3), the linear fissure-and-fault

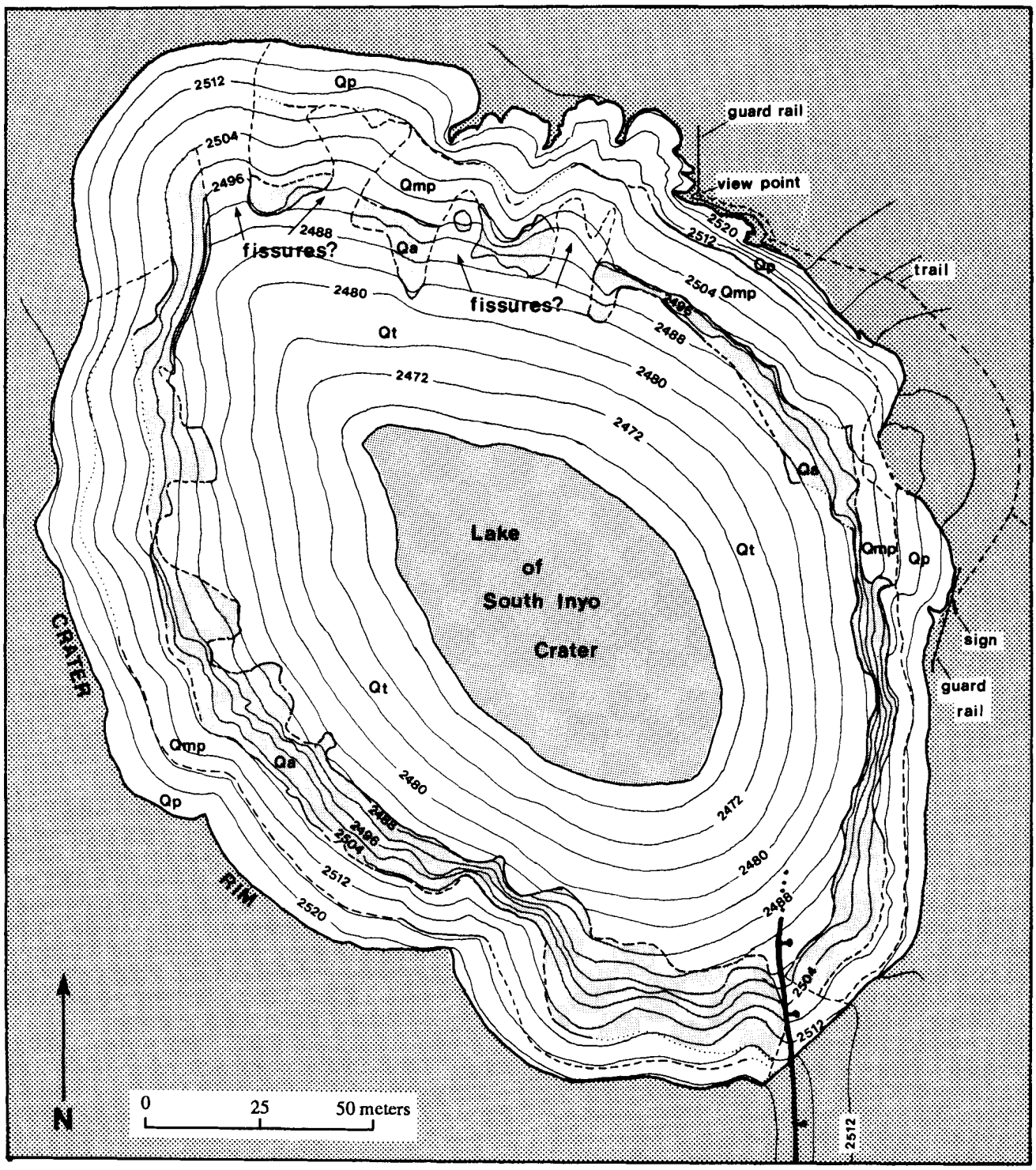

Fig. 4. Map of South Inyo Crater. Mapped units are andesite lava flows and interflow breccias (*Qa*), pre-Inyo Craters mafic pyroclastic deposits (*Qmp*), South Inyo Crater phreatic debris (*Qp*), and talus or slope wash (*Qt*). Elevation is in meters

topography has been partly obscured by deposition of up to a few meters of primarily ash-sized debris around a circular vent.

The easternmost cluster of vents includes the Inyo Craters, Summit Crater, and North Deer Mountain Crater (Fig. 3). This set lies within a north-south trend of normal faults and fissures which roughly parallels the Inyo trend and is thought to be the surface expression of one of the dike segments that fed the Inyo chain (Pollard et al. 1984; Fink 1985; Mastin and Pollard 1988). The proximity of several older eruptive vents on or near this trend (black triangles, Fig. 3) indicates that this has been a site of previous, perhaps repeated, eruptive activity. In particular, the eruption of Summit

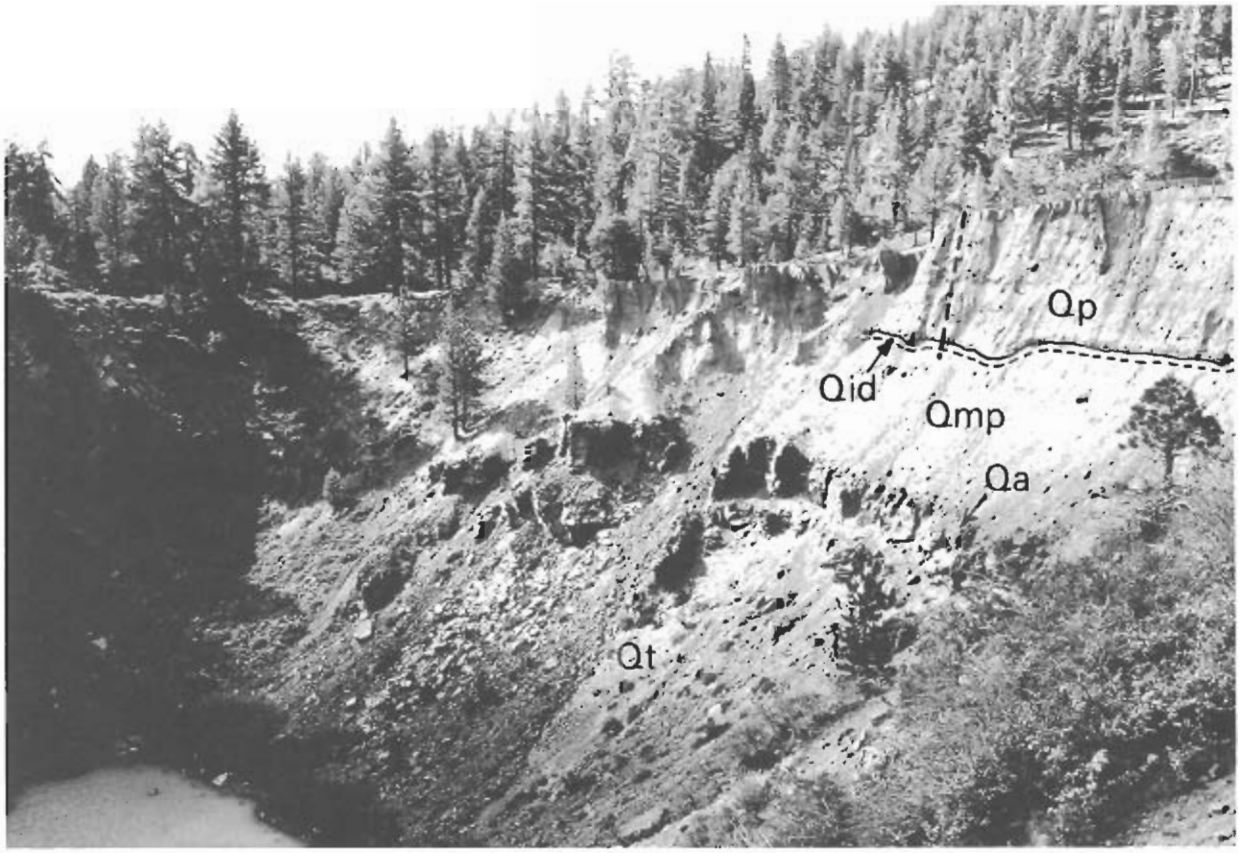

Fig. 5. Northeast wall of South Inyo Crater. *Qt*, talus and slope wash; *Qa*, andesite flows; *Qmp*, basalt pyroclastic deposits; *Qid*, rhyolite air-fall units; *Qp*, phreatic debris. The *dashed, sub-vertical line* denotes the location of the stratigraphic column and sample locations in Fig. 6

Crater exploited the older vent of Deer Mountain dome, and there is evidence (described later) that the South Inyo Crater eruption utilized an older basaltic vent.

South Inyo Crater is by far the largest and most spectacular crater in this area. Its volume below the elevation of the pre-eruptive ground surface (9.0×10^5 m^3) exceeds that of both North Inyo Crater (5×10^5 m^3) and Summit Crater (1.5×10^5 m^3). South Inyo Crater is approximately rhombohedral in shape, with sides oriented parallel to the two prominent fissure and fault sets that intersect in this area, suggesting that the crater attained its present form by collapse of debris into the vent along fissures that were older (perhaps by only a few hours or days) than the eruption itself. Evidence of such fissuring is manifest in places within the crater. Andesite flows a few meters thick are continuous around the crater wall except on the southeast corner, where an east-side-down normal fault displaces andesite and phreatic debris (Fig. 4), and on the north side, where four breaks in the andesite cliff may be eroded fissures.

There is some evidence that this has been the site of at least one previous eruption involving magma and groundwater. Overlying the lava flows are 8 to 12 m of red mafic pyroclastic debris (Qmp, Figs. 4 and 5) which consists primarily of ash with minor scoriaceous lapilli. This deposit is less than 1 m thick in fault scarps 200 m west and south of South Inyo Crater, suggesting that its source vent was nearby - perhaps at the present site of South Inyo Crater. Indistinct cross beds near the base of Qmp suggest that part of it was deposited by surges and may be phreatomagmatic in origin. The uppermost 1 to 2 m of the deposit is weathered, and an accumulation of charred pine needles and wood fragments at the upper contact indicate that it was exposed for some time before subsequent depositional events.

Above the mafic pyroclastic deposit lies approximately 1 cm of fine, white rhyolitic ash from a 600-yr-B.P. eruption at Mono Craters (Wood 1977; Sieh and Bursik 1986), approximately 1.1 m of unconsolidated pumice lapilli from the South Deadman vent, and approximately 1 cm of pumice lapilli from the Glass Creek vent (C. D. Miller, written communication 1988). These deposits (collectively labelled Qid in Fig. 5) are not delineated in Fig. 4 due to poor exposure. They are absent in shovel pits dug on the southeast and west sides of the crater wall, probably due to slumping of the crater wall during the eruption. The eruptive debris from South Inyo Crater (Qp, Figs. 4 and 6) overlies the rhyolitic pumice-fall deposits and was laid down before any significant weathering or soil had developed on them.

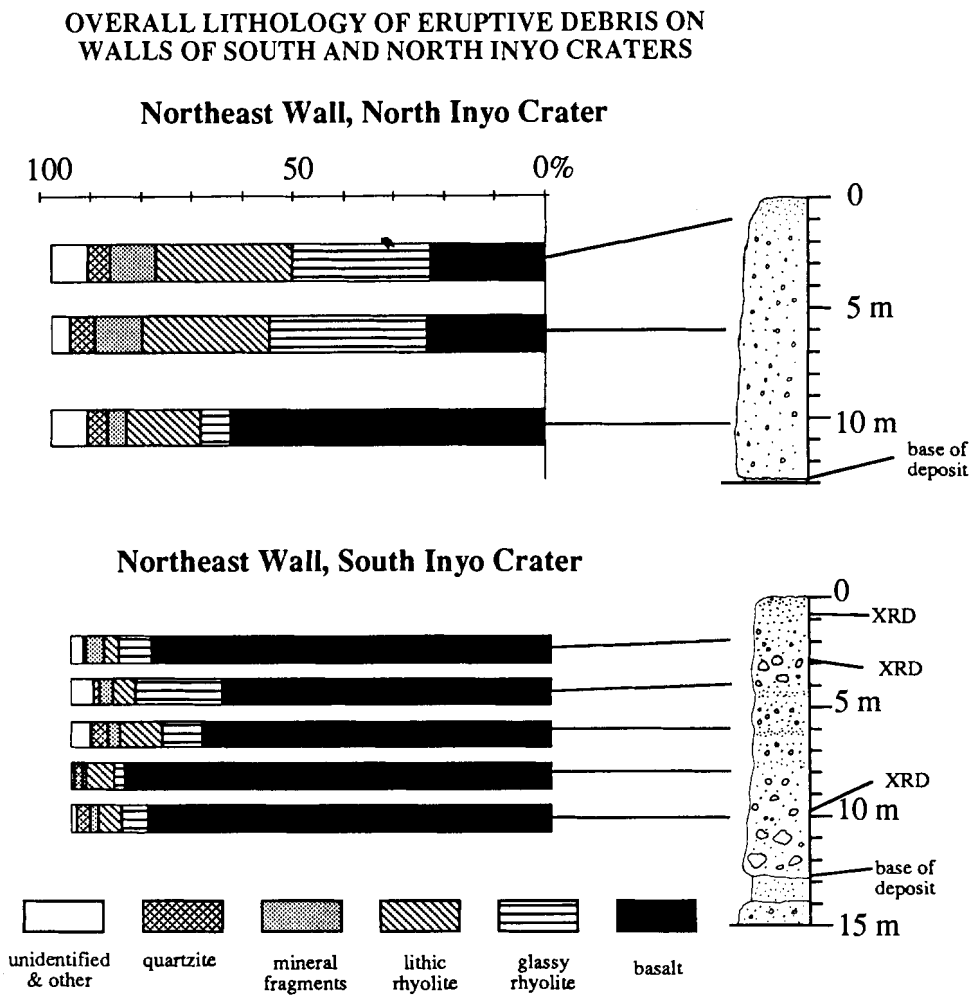

Fig. 6. Overall lithology versus stratigraphic position in the eruptive deposits from North Inyo Crater (*top*) and South Inyo Crater (*bottom*), *XRD* indicates locations where x-ray diffraction samples were taken

The eruptive deposits

The deposits of the phreatic craters consist of medium gray-brown to very light gray, variably indurated, unaltered accumulations of accidental clasts from the underlying stratigraphy supported in a matrix of ash-sized debris. The phreatic debris can be distinguished from the underlying pumice-fall by its silty matrix which drains poorly and produces fine drainage textures on steep slopes. The deposits range in thickness from a few meters at the crater walls (13 m maximum at South Inyo Crater) to a thickness small enough at 200–1000 m distance that most of the debris has washed into the underlying pumice. The areal patterns of the deposits in the central and western clusters of craters in Fig. 3 are roughly circular in map view, whereas those from the eastern set extend as lobes at least a kilometer to the northeast.

The eruptive deposit from South Inyo Crater has been mapped separately from the others (Fig. 3). The volume of the deposit was estimated by measuring the thickness of the deposit in shovel pits at several places around the crater (numbered points, Fig. 3) and drawing isopachs in different ways around these points. The volume estimate, between 0.8 and 1.2×10^9 m^3, is roughly equal to the volume of the crater. Thus the crater was probably created by the South Inyo Crater eruption and not by an earlier eruption of the mafic pyroclastic deposit that underlies the South Inyo Crater debris.

Deposits from the two Inyo Craters and from Summit Crater overlap one another and can be distinguished from each other by lithologic differences. Stratigraphic relationships exposed on the east side of Deer Mountain show that Summit Crater – the northernmost of these three – was the first to erupt, followed by North Inyo Crater, and finally by South Inyo Crater. The three deposits are separated by two gradational zones which are thin (a few to several centimeters) relative to the thickness of each deposit at this outcrop (50 cm to 2.5 m), suggesting that each eruption started before the preceding one had completely stopped, but that each had nearly stopped before the following one commenced.

In all exposures, the phreatic deposits are massive to coarsely plane-parallel bedded, with bedding generally tens of centimeters to more than a meter thick. Cross bedding and scour-and-fill structures, which are typical of surge deposits, have not been observed, although the abundance of water in these eruptions and their appar-

Table 1.
Summary of Point Count Data

Sample	Location	Points counted	Basaltic rocks	Rhyolite glass	Early rhyolite	Mineral fragments	Meta-morphic	Pumice[a]	Unid. and other
Deposit from South Inyo Crater									
2 ft, NE, SIC	0.61 m below rim, NE wall, S. Inyo Crater	400	79%	9%	7%	2%	1%	0%	2%
4 ft, NE, SIC	01.22 m below rim, NE wall, S. Inyo Crater	400	69%	14%	8%	5%	3%	0%	1%
2.0 m, NE, SIC	2.0 m below rim, NE wall, S. Inyo Crater	400	60%	18%	6%	9%	0%	0%	7%
10 ft, NE, SIC	3.05 m below rim, NE wall, S. Inyo Crater	400	59%	19%	11%	5%	5%	0%	1%
4.0 m, NE, SIC	4.0 m below rim, NE wall, S. Inyo Crater	400	41%	37%	7%	6%	0%	0%	9%
16 ft, NE SIC	4.87 m below rim, NE wall, S. Inyo Crater	400	52%	25%	11%	5%	4%	1%	2%
6.0, NE, SIC	6.0 m below rim, NE wall, S. Inyo Crater	400	46%	26%	15%	8%	0%	0%	5%
8.0, NE, SIC	8.0 m below rim, NE wall, S. Inyo Crater	400	60%	21%	9%	5%	1%	0%	4%
10.0 m, NE, SIC	10.0 m below rim, NE wall, S. Inyo Crater	400	50%	23%	12%	7%	2%	0%	4%
36 ft, NE, SIC	11.0 m below rim, NE wall, S. Inyo Crater	400	50%	15%	9%	19%	4%	0%	3%
4.0 m, SW, SIC	4.0 m below rim, SW wall, S. Inyo Crater	400	53%	21%	13%	8%	2%	0%	3%
4.2 m, NE, NIC	4.2 m below rim, NE wall, N. Inyo Crater	400	45%	15%	16%	18%	3%	0%	3%
sample 202	270 m east of S. Inyo Crater	400	44%	30%	13%	7%	4%	1%	1%
sample 207b	600 m NE of S. Inyo Crater	400	55%	11%	8%	15%	7%	0%	4%
sample 206a[b]	1280 m NE of S. Inyo Crater	400	17%	17%	6%	17%	5%	34%	4%
Deposit from North Inyo Crater									
6.0 m, NE, NIC	6.0 m below rim, NE wall, N. Inyo Crater	400	17%	30%	30%	10%	5%	0%	8%
11.0 m, NE, NIC	11.0 m below rim, NE wall, N. Inyo Crater	400	24%	32%	26%	10%	5%	0%	3%
15.0 m, NE, NIC	15.0 m below rim, NE wall, N. Inyo Crater	400	38%	19%	21%	12%	2%	2%	6%
Deposit from Summit Crater									
Summit Crater rim	Top of Deer Mountain	400	4%	24%	20%	36%	3%	11%	2%
From elsewhere									
Middle crater	470 m NW of S. Inyo Crater	400	6%	60%	14%	11%	3%	3%	3%
North Deer Mtn Crater	North side of Deer Mountain	400	2%	61%	16%	17%	3%	0%	1%
Sample 209[c]	East side of Deer Mountain	400	36%	20%	13%	14%	5%	10%	2%

[a] Includes pumiceous Deer Mountain rhyolite
[b] The high pumice content in this sample suggests that the phreatic debris has mixed with the underlying pumice airfall
[c] Probably a mixture of Inyo Craters and Summit Crater deposits

Table 1 (continued)
Summary of Lapilli Count Data

Sample	Location	Number counted	Basaltic rocks	Lithic early rhyolite	Glassy rhyolite	Metamorphic, granitic	Miscellaneous volcanic	Unidentified
South Inyo Crater deposit								
2.0 m, NE, SIC	2.0 m below rim, NE wall, S. Inyo Crater	218	95%	3%	0%	1%	1%	0%
4.0 m, NE, SIC	4.0 m below rim, NE wall, S. Inyo Crater	372	87%	3%	1%	4%	3%	2%
6.0, NE, SIC	6.0 m below rim, NE wall, S. Inyo Crater	475	77%	9%	0%	8%	0%	6%
8.0, NE, SIC	8.0 m below rim, NE wall, S. Inyo Crater	448	87%	9%	0%	3%	0%	1%
10.0 m, NE, SIC	10.0 m below rim, NE wall, S. Inyo Crater	332	89%	5%	0%	6%	0%	0%
2.0 m, SW, SIC	2.0 m below rim, SW wall, S. Inyo Crater	218	90%	3%	0%	4%	2%	1%
4.0 m, SW, SIC	4.0 m below rim, SW wall, S. Inyo Crater	329	87%	8%	0%	5%	0%	0%
4.2 m, NE, NIC	4.2 m below rim, NE wall, N. Inyo Crater	392	72%	10%	0%	10%	4%	4%
202	270 m east of S. Inyo Crater	433	74%	18%	0%	6%	2%	0%
204	230 m east of S. Inyo Crater	337	76%	17%	1%	5%	2%	0%
North Inyo Crater deposit								
11.0 m, NE, NIC	11.0 m below rim, NE wall, N. Inyo Crater	314	50%	30%	0%	16%	0%	3%
15.0 m, NE, NIC	15.0 m below rim, NE wall, N. Inyo Crater	400	62%	16%	0%	6%	6%	11%
Deer Mountain Crater Deposit								
Summit Crater	Top of Deer Mountain	305	32%	5%	2%	11%	47%	3%

Table 2. Grain-Size distributions phi size

Sample	Sample Location	< −8 weight fraction	−8 to −7 weight fraction	−7 to −6 weight fraction	−6 to −4.25 weight fraction	−4.25 to −3.75 weight fraction	−3.75 to −2.75 weight fraction	−2.75 to −2 weight fraction	−2 to −1 weight fraction	−1 to 0 weight fraction	0 to 1 weight fraction	1 to 2 weight fraction	2 to 3 weight fraction	3 to 4 weight fraction	> 4 weight fraction	Median (phi)	Sigma (phi)
From South Inyo Crater Deposit																	
2.0 m, NE, SIC	2.0 m below top, NE wall, S. Inyo Crater	0.000	0.086	0.062	0.048	0.033	0.063	0.032	0.061	0.045	0.070	0.046	0.046	0.039	0.368	0.49	> 5.1
4.0 m, NE, SIC	4.0 m below top, NE wall, S. Inyo Crater	0.000	0.080	0.045	0.042	0.020	0.047	0.030	0.090	0.060	0.097	0.062	0.060	0.052	0.315	0.81	> 4.37
6.0 m, NE, SIC	6.0 m below top, NE wall, S. Inyo Crater	0.000	0.025	0.017	0.144	0.035	0.112	0.090	0.123	0.080	0.087	0.034	0.029	0.027	0.195	−1.70	> 4.38
8.0 m, NE, SIC	8.0 m below top, NE wall, S. Inyo Crater	0.000	0.000	0.000	0.313	0.123	0.188	0.050	0.138	0.035	0.027	0.012	0.010	0.010	0.092	−3.76	2.03
10.0 m, NE, SIC	10.0 m below top, NE wall, S. Inyo Crater	0.082	0.054	0.008	0.186	0.043	0.082	0.050	0.092	0.052	0.058	0.030	0.028	0.026	0.208	−2.64	> 4.94
2.0 m, SW, SIC	2.0 m below top, SW wall, S. Inyo Crater	0.051	0.068	0.069	0.447	0.064	0.074	0.029	0.021	0.014	0.022	0.012	0.012	0.010	0.108	−5.81	3.54
4.0 m, SW, SIC	4.0 m below top, SW wall, S. Inyo Crater	0.096	0.026	0.028	0.168	0.029	0.060	0.027	0.056	0.036	0.056	0.038	0.042	0.036	0.302	−0.71	> 5.18
4.2 m, NE, NIC	4.2 m below top, NE wall, N. Inyo Crater	0.031	0.000	0.013	0.077	0.068	0.229	0.236	0.051	0.028	0.036	0.025	0.027	0.025	0.153	−2.49	3.85
204	230 m east of S. Inyo Crater	0.000	0.000	0.000	0.179	0.033	0.104	0.052	0.143	0.076	0.099	0.057	0.065	0.040	0.153	−1.55	4.09
202	270 m east of S. Inyo Crater	0.000	0.000	0.000	0.168	0.089	0.126	0.087	0.052	0.161	0.038	0.053	0.047	0.036	0.142	−1.89	3.84
206b	890 m NE of S. Inyo Crater	0.000	0.000	0.000	0.000	0.000	0.000	0.155	0.130	0.091	0.153	0.106	0.100	0.077	0.188	0.31	> 3.19
205	1100 m NE of S. Inyo Crater	0.000	0.000	0.000	0.000	0.000	0.000	0.011	0.037	0.055	0.162	0.136	0.116	0.086	0.397	2.34	> 2.08
From North Inyo Crater Deposit																	
6.0 m, NE, NIC	6.0 m below top, NE wall, N. Inyo Crater	0.000	0.002	0.004	0.020	0.040	0.049	0.046	0.043	0.036	0.076	0.067	0.070	0.056	0.492	3.86	> 3.00
11.0 m, NE, NIC	11.0 m below top, NE wall, N. Inyo Crater	0.000	0.000	0.000	0.000	0.007	0.036	0.030	0.046	0.037	0.067	0.064	0.075	0.079	0.559	> 4	> 2.03
15.0 m, NE, NIC	15.0 m below top, NE wall, N. Inyo Crater	0.000	0.000	0.000	0.128	0.047	0.191	0.058	0.085	0.062	0.039	0.034	0.045	0.039	0.271	−1.11	> 3.95
From Elsewhere																	
Middle Crater	Top of est rim, Middle Crater	0.000	0.000	0.000	0.000	0.000	0.026	0.054	0.092	0.099	0.161	0.108	0.074	0.038	0.349	1.64	> 2.56

ent explosiveness (suggested by the abundance of large blocks thrown out of South Inyo Crater) suggests that, like many phreatic and phreatomagmatic eruptions (Fisher and Schmincke 1984, p. 247), they may have involved surges. None of the phreatic deposits contain any sharp contacts between bedding planes which would suggest a pause in any eruption.

On the northeast wall of South Inyo Crater (Fig. 5) the deposit consists of a single fining-upward sequence with an accumulation of large blocks near its base, suggesting that the eruption began with great intensity and diminished with time. In the uppermost 2 m of the deposit, accretionary lapilli (suggesting condensed steam) appear, then grade upward into a thoroughly cemented ground mass which contains irregularly shaped vesicles about 1 mm in diameter. Sulfur coatings on crack walls in the ground mass in the uppermost meter may have been deposited by sulfur-laden steam emitted from the crater during or after the eruption, or perhaps by sulfurous vapor streaming upward through the hot deposit.

The lithology and size distribution of the eruptive debris in the walls of North and South Inyo Craters were determined (Tables 1, 2) by taking large (5–10 kg) samples at points on the crater walls, sieving the debris, and making statistical counts of lapilli- and coarse ash-sized fragments. The lithology and size distribution of large blocks in the crater wall were determined by rappelling down the crater walls, and noting the maximum and minimum diameters, lithology, and position below the rim of each block larger than 5 cm diameter within a 2-m-wide vertical strip. All blocks counted in these measurements were basalt.

The lithologic characteristics of each stratigraphic unit in the subsurface (down to at least 500 m depth) are quite distinct, and allowed the depth of origin of more than 90% of the fragments in the deposit to be inferred with a fair degree of confidence. The criteria used to assign depths of origin to each lithology are listed in Table 3. The lithology of the debris smaller than 0.06 mm diameter was too small to identify quantitatively, but x-ray diffraction studies show that most of this debris consists of sanidine, anorthite, pyroxene, olivine, quartz, and glass; they are of the same mineralogy, and presumably come mostly from the same sources, as the larger particles. No minerals of obvious geothermal origin (e.g. zeolites, opal, quartz fracture fillings) have been identified.

The variation in lithology with stratigraphic position in the Inyo Craters deposits is illustrated in Fig. 6. Fragments are present from stratigraphic units at least as deep as the devitrified part of the early rhyolite flow at 458 m depth. Clasts may also have come from greater depth, but this cannot be confirmed because all lithologies present at greater depth are also present at shallower depth. Additional lithologic data in Table 1 indicate that debris from the deepest identifiable source, the early rhyolite lava, is present even at the very base of the South Inyo Crater deposit, and near the base of the North Inyo Crater deposit. Thus, each eruption was tapping debris from at least 458 m depth at or near its inception, probably along open fractures. Nevertheless,

Table 3.

Major lithologies in the South Inyo Crater deposit	Inferred origin
Basalt, andesite, and plagioclase fragments	Basalt above 305 m depth
(a) Volcanic rocks that can't be correlated with specific volcanic units, including black obsidian and aphanitic fragments with biotite or hornblende phenocrysts, (b) granitic and metamorphic fragments, (c) quartz, hornblende, and biotite fragments	Gravels below basalt, 304–358 m depth
Aphyric glass, commonly vesicular	Assigned to early rhyolite tuff, 358–412 m depth, but may contain some surficial South Deadman Flow tephra. May also include a juvenile fraction
Rhyolite glass with elongate microlites of plagioclase(?) and perlitic fractures	Perlitic carapace on top of early rhyolite flow, 412–~458 m depth
Lithic rhyolite with detached flow bands, leached plagioclase phenocrysts, or a spherulitic texture in thin section	Interior of early rhyolite flow, ~458 m to between 577 and 627 m depth

like many phreatomagmatic deposits (e.g. Wohletz and Sheridan 1983), the percentage of shallowly derived debris (i.e. basalt and andesite) in the overall lithology of the the North Inyo Crater deposit (Fig. 6) decreases from the base to the top, indicating an overall reaming of material from lesser to greater depths as the eruption progressed. A similar pattern is evident in the lowermost two thirds of the South Inyo Crater stratigraphy. However in the uppermost third of this deposit the trend reverses. This reversal coincides with a decrease in average bedding thickness and grain size. It is inferred that these layers were deposited in the waning stages of the eruption when debris from the crater walls periodically sloughed into the vent and was spasmodically expelled, as has been observed in some maar-type eruptions (e.g. Self et al. 1980).

Volume of debris tapped from each depth

The availability of subsurface information from the drill core, and the quantitative information on lithology and grain-size distribution make it possible to estimate the volume of material derived from each depth in the Inyo Craters ejecta.

For the South Inyo Crater deposit, the overall lithology was estimated by taking samples at the crater wall and at points away from the crater (shown in Fig. 3), and determining the grain-size distribution and lithology from sieve analysis. Lithology and size distribution of blocks larger than 20 cm diameter were determined at points away from the crater wall by staking out plots along two radial lines in the upwind direction west and

Table 4
Average grain-size distributions

phi size	>4	4	3	2	1	0	−1	−2	−2.75	−3.75	−4.25	−6	−7	−8
South Inyo Crater	0.273	0.040	0.051	0.053	0.073	0.052	0.070	0.045	0.072	0.042	0.147	0.025	0.037	0.020
North Inyo Crater	0.441	0.058	0.064	0.055	0.061	0.045	0.058	0.045	0.092	0.031	0.049	0.001	0.001	0.000

Average lithology of grains larger than 0.06 mm diameter

	Basalt	Rhyolite glass	Early rhyolite	Quartz, hornblende	Feldspars	Metamorphics, granitics	Miscellaneous volcanics	Pumice	Unidentified, other
South Inyo Crater	73%	8%	9%	1%	2%	4%	1%	0%	2%
North Inyo Crater	46%	14%	22%	3%	2%	6%	1%	0%	6%

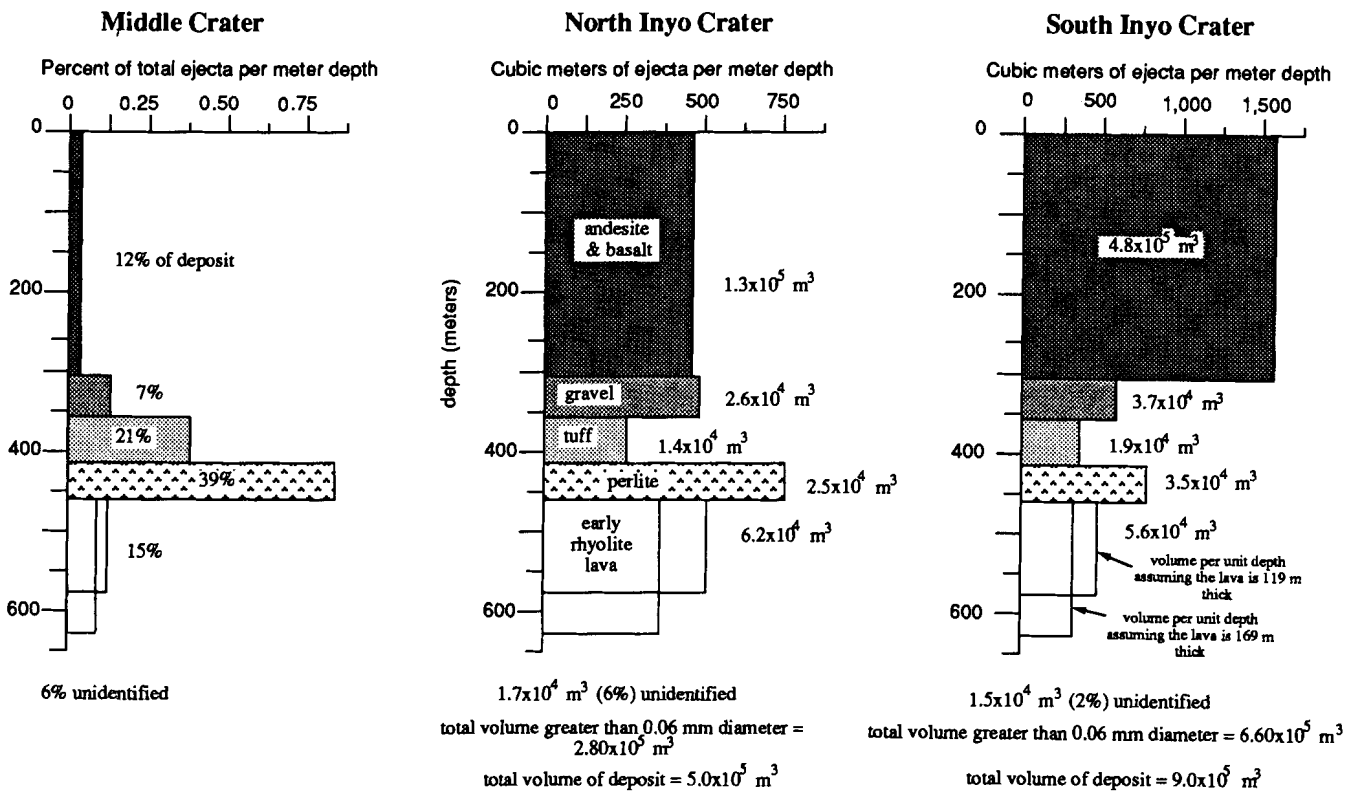

Fig. 7. Plot of the volume of phreatic debris per meter depth as a function of depth for ejecta from North and South Inyo Craters and Middle Crater

south of the crater, where the blocks were (beyond about 200 m from the crater rim) not covered by fine debris. The lithology and size distribution of the blocks was determined by measuring the maximum and minimum diameter of each block larger than 20 cm in diameter, and noting its lithology. The overall lithology (Table 4) was determined by combining the lithologic results with the grain-size distribution data. The lithology of the fragments smaller than 0.06 mm diameter, which represent 27% of the deposit, could not be determined quantitatively.

For North Inyo Crater the overall lithology (Table 4) was estimated from three samples from the crater wall. The total volume of the deposit was assumed to equal the volume of the crater below the base of the phreatic debris.

At Middle Crater, no cross sectional exposures of the deposit exist from which variations in grain size or lithology could be observed. However surface observations and one grain-size analysis (Table 2) of the debris from the crater rim indicate that the deposit consists mostly of ash-sized fragments. The lithologies were estimated from a point count of this ash-sized debris (Table 1).

Figure 7 shows rough estimates of the volume of material derived as a function of depth for the Inyo Craters deposits and for Middle Crater. For the South Inyo Crater deposit, the volume of debris from the conglom-

erate at 304–358 m depth corresponds to a cylinder about 27 m in diameter, or a 100-m-long slot 6 m wide. For the perlite and flow-banded early rhyolite lava, the erupted volumes correspond to cylinders 31 m and 22–30 m in diameter, or 100-m-long slots 6 m and 3.3–7 m wide, respectively. By comparison, the thickness of the largest breccia encountered in the drill core (within the early rhyolite flow) was approximately 17 m (Eichelberger et al. 1988; and Fig. 2 of this paper).

Studies of maars and diatremes in Germany (Lorenz 1973, 1986) and Scotland (Whyte 1968) suggest that the conduits to phreatomagmatic eruptions are widened by the slumping or faulting of wall rock. If the horizontal distance between the outer margins of the two outermost breccia zones (approximately 37 m) represents the conduit with two large slide blocks, the conduit width would be about 1.2 to 10 times that resulting from the excavation of the erupted debris alone (assuming conduit geometries ranging from a 100-m-long tabular to a cylindrical body). If the largest breccia alone represents the conduit (as shown in Fig. 2), its thickness would be approximately 1 to 4.5 times that resulting from the excavation of the erupted debris. In either case, the conduit width was probably not more than an order of magnitude wider than that of the void created by removal of the erupted debris (although over a greater thickness some slumping may have occurred in the wall rock that cannot be seen in the drill core).

Each of these eruptions selectively removed the finest, most poorly indurated debris from the subsurface. At South Inyo Crater, most of the pre-eruptive volume of the crater consisted of massive flows made up of blocks more than 25 cm in diameter. By contrast, blocks greater than 25 cm diameter make up only about 2% of the volume of the deposit. Most of the large blocks that occupied this volume must have fallen down the conduit when the smaller debris was removed. This is borne out by the drilling results, which show that the center of the largest breccia below the crater contains a concentration of basalt clasts (up to 50% by volume; Eichelberger et al. 1988), while the margins of the breccia contain mostly rhyolite, much of which is wall rock from nearby depths. The basalt in the breccia lies near the primitive end of an SiO_2 versus MgO trend that characterizes basaltic rock from the uppermost 305 m depth (Eichelberger et al. 1988), suggesting to this author that that it fell down the vent from the lower part of the basalt stratigraphy. Alternatively, Eichelberger et al. (1988) suggest that it may be an old intrusion which remained in the center of the eruptive vent as material was intruded on both sides of it.

The North Inyo Crater deposit contains relatively less basalt and more early rhyolite than the South Inyo Crater deposit. The Middle Crater deposit, which probably erupted through the same thick sequence of basalt, contains almost no basaltic debris (Table 1, Fig. 7) and abundant early rhyolite tuff and perlitic fragments. The difference in lithology coincides with a general decrease in average grain size from the largest to the smallest crater. Both of these differences probably reflect a general decrease in the eruptive velocities and therefore the carrying capacity of the eruptive column; the smallest eruption could remove only the smallest and most poorly indurated debris from the vent walls.

Velocity of the South Inyo Crater eruption

In order to quantify the strength of the eruption of South Inyo Crater, the eruptive velocity was estimated from the distance large blocks were thrown from the crater center. Several attempts have been made by various authors to relate eruptive velocity to the ejected distance of large blocks (e.g. Minakami 1942; Gorshkov 1959; Lorenz 1970; Fudali and Melson 1972; Self et al. 1980). For this study the eruptive velocity was determined using an analytical solution by Minakami (1942), presented in a distilled form in Self et al. (1980), which is derived from an approximation of the differential equations that govern the forces of gravity and air drag on a ballistically ejected block. The solution (described in detail in the appendix) relates the distance travelled by the block (X_m) to the initial velocity (u_o), the initial trajectory angle of the block measured from horizontal (θ), the block's radius (r), density (ρ_r), and drag coefficient (C_D), the tail wind velocity (W), the air density (ρ_a), and the vertical distance (ξ) of the crater center below the landing point. Values of θ, ρ_r, C_D, W, ρ_a, and ξ used in this study are given in Table 5. The relationship between X_m and u_o for different block sizes is graphed in Fig. 8. It is important to note that, for a given velocity, large blocks travel farther than small blocks due to their greater mass to surface area ratio. Velocity estimates for small blocks therefore are higher than those for larger blocks at the same distance from the crater.

The solution above assumes (1) that the block's trajectory is short enough that the air density and the direction and strength of the Earth's gravitational field don't change with position, and (2) that Newton's drag law is applicable; that is, that the drag force on the block is proportional to the square of the block's velocity. The solution also assumes that the air around the block has no velocity in the vertical direction. The latter assumption is the most problematic because the block

Table 5. Parameters used in ballistic analysis

Variable	Value	Commens
C_d	1.0	
ρ_a	0.884 kg/m^3	Density of dry air at 25° C and ambient pressure at 2500 m altitude
ρ_r	2200 kg/m^3	Approximate density of sparsely vesicular andesite
W	0 m/s	
ξ	−40 m	Slightly less than the present depth of South Inyo Crater
θ	45°	Ejection angle that gives the greatest range for a given velocity (see Appendix B for an explanation)

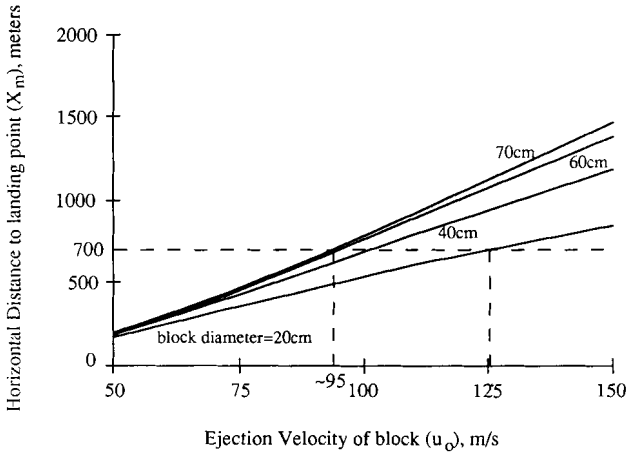

Fig. 8. Range (X_m) versus ejection velocity (u_o) for blocks ejected in still air, using the equations given in the appendix, and block and air properties shown in Table 5

probably left the vent within a rising stream of gas and debris. Self et al. (1980) used a numerical solution to test this assumption under conditions where r = 10–20 cm, $u_o = 100$ m/s, $\xi = 0$, and where θ, ρ_r, C_D, W, and ρ_a, are as given in Table 5. For blocks ejected within a gas stream whose velocity diminished from that of the blocks at the vent to zero within 10 to 100 m from the vent, they found that X_m could be 30% to 40% greater than that estimated from the equations by Minakami (1942). For larger blocks, the frictional drag is less significant and the error is therefore smaller. In this study the distance of the outermost blocks from the crater center is used to estimate the maximum eruptive velocity. The errors introduced by the uncertainty in θ and the vent velocity, however, have opposite effects on the calculated result. Estimating the eruptive velocity from the distance travelled by the outermost blocks therefore gives neither a maximum nor a minimum value for the maximum vent velocity, but rather a ballpark figure that is probably correct to within a few tens of percent.

At Inyo Craters, blocks ranging from 20 to 70 cm in diameter were thrown at least 700 m from the crater center (horizontal dashed line, Fig. 8), indicating that they were expelled at a velocity of 95 to 125 m/s. The velocity (calculated from Minakami's equation) required to throw a 1-m-diameter block from the bottom of the crater to the rim is about 40 m/s, one third to one half that of some of the fastest blocks. The velocities of the larger blocks are similar to those calculated from photographs and from direct observations of the 1976–1977 phreatic eruptions of La Soufriere de Guadeloupe (30 to 150 m/s, Le Guern et al. 1980) and to velocities calculated form ballistic studies of the ejecta from the 1977 eruptions of Ukinrek Maars, Alaska (100 ± 20 m/s, Self et al. 1980).

A second objective of this ballistic study was to get some insight into the explosiveness of the eruption from the distribution of blocks around the crater. Similar studies at other volcanoes suggest that explosive and non-explosive eruptions (or eruptive phases) are characterized by different block-size distributions. The initial phases of extremely explosive eruptions (e.g. Arenal volcano in 1968 (Fudali and Melson 1972) and Ukinrek Maars, Alaska (Self et al. 1980)) have been known to produce deposits in which the average block size increases with distance from the crater. This distribution is hypothesized to be caused by expulsion of blocks of a variety of sizes at the same velocity through still air. Due to the reduced effect of air drag on large blocks, they travel farther than the smaller ones. More sustained eruptions have been known to produce deposits in which the average block size decreases with distance (e.g. Lorenz 1970; Self et al. 1980). In these eruptions, it is hypothesized that debris is supported within a gas stream and decouples after a time which is dependent on its terminal velocity and angle of ejection. The larger blocks drop out of the eruptive stream more quickly than the smaller ones and therefore attain a shorter range.

At distances more than about 350 m from the center of South Inyo Crater, semi-log plots of block-size distribution versus distance (Fig. 9) show a roughly linear decrease for all size ranges (block-size distributions

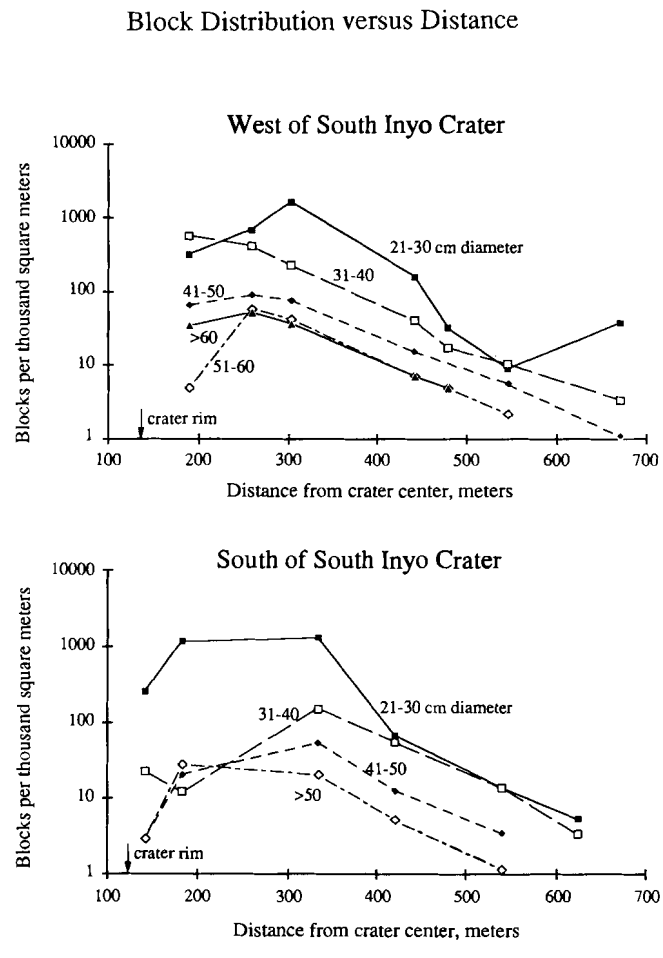

Fig. 9. Number of blocks per 1000 m^2 as a function of distance from the center of South Inyo Crater. (*top*) Block distribution versus distance west of South Inyo Crater. (*bottom*) Block distribution versus distance south of South Inyo Crater

within 350 m of the crater center are affected by debris cover and the influence of small, directed blasts, and are ignored). Furthermore, the slope of each line in these plots is nearly the same for all block sizes, suggesting that no particular block size decreases in abundance more quickly than any other. Thus the average block size does not increase as it does for some of the explosively produced deposits around Arenal and the Ukinrek Maars. On the other hand, neither does it decrease (although this may be because the block distribution was measured in the upwind direction from the crater). It seems likely that the blocks around the crater were dropped during both an initial explosive phase of the eruption and during later phases, i.e. that the observed block-size distribution may have resulted from some combination of the two processes described above.

Energy of the South Inyo Crater eruption

The energy of the eruption of South Inyo Crater can only be evaluated very approximately due to the fact that most forms of energy released during the eruption left no physical evidence of their existence. The primary energy source of most volcanic eruptions comes from the cooling and solidification of magma (Yokoyama 1956, 1957; Nakamura 1964), but the energy that drove the phreatic eruptions at Inyo Craters, like most geysers and hydrothermal eruptions, was probably contributed by cooling and expansion of water and steam from subsurface pressure and temperature conditions to ambient pressure at 100° C or less (White 1955; Le Guern et al. 1980). Less important forms of energy, including acceleration and lifting of fluid and ejecta, ground shaking, shock waves in the atmosphere, and some rock breakage, probably are powered by the expansion, cooling, and condensation of steam and water.

At South Inyo Crater, the kinetic energy ($E_{k,debris}$) of the erupted ejecta can be obtained from the mass (m) of erupted debris (i.e. the volume of the South Inyo Crater deposit times typical rock density),

$$(\sim 0.9 \times 10^6\ m^3) \cdot (\sim 2200\ kg/m^3) = \sim 2.0 \times 10^9\ kg$$

and average velocity estimates (u_o) of 50–100 m/s. Using these values,

$$E_{k,debris} = \frac{1}{2} m u_0^2 = \frac{1}{2} (2.0 \times 10^9\ kg)$$

$$(50\text{–}100\ m/s)^2 = 0.25\text{–}1.0 \times 10^{13}\ Joules$$

In a study of the eruptive energy of geysers in the western USA, White (1955) noted that the kinetic energy of water and steam in these eruptions ($E_{k,steam}$), estimated by the height of geyser plumes, is a few tenths of a percent of the total energy (E_{tot}) released by cooling and expansion of the water from boiling-point pressure and temperature at a given depth to 100° C and ambient pressure at the surface. If, as probably occurs in phreatic eruptions, a part of the kinetic energy of the rising steam and water were imparted to blocks and debris, the ratio $E_{k,debris}/E_{tot}$ in phreatic eruptions would probably be somewhat smaller than the ratio $E_{k,steam}/E_{tot}$ observed in geyser eruptions; i.e. ratios of $E_{k,debris}/E_{tot}$ would approach 10^{-3}. Similar estimates of energy from phreatic eruptions at La Soufrière de Guadeloupe (Le Guern et al. 1980) support this hypothesis. Le Guern et al. (1980) estimated ratios ($E_{k,debris}/E_{therm}$) of kinetic energy of ejecta to the thermal energy of water and steam from approximately 1.1×10^{-3} to 1.1×10^{-2}, not far off the estimates of $E_{k,steam}/E_{tot}$ by White (1955).

If one assumes that the ratio of $E_{k,debris}/E_{tot}$ of the South Inyo Crater eruption lay within the range of $E_{k,debris}/E_{therm}$ given by Le Guern et al. (1980), one would estimate an energy for the eruption of:

$$E_{tot} \approx 2.3 \times 10^{14} - 9.0 \times 10^{15}\ Joules$$

This energy is equivalent to that given off by the solidification and cooling of $.071\text{–}2.8 \times 10^6$ m^3 of rhyolitic magma from 900° C to 25° C (assuming a heat of fusion of $\Delta H_f = 0.7 \times 10^9$ J/m^3 and heat capacity $\rho C_p = 3 \times 10^6$ $J/m^3\,°K$; where ρ = rock density and C_p = specific heat at constant pressure, Williams and McBirney 1979, p. 29). Such a volume of magma would make up a dike 2–90 m thick, as long in north-south dimension as South Inyo Crater, which extended vertically from the top of the basement to the deepest point at which the breccia was encountered in the drill core. Alternatively, if one assumed that all the magma responsible for the eruption was fragmented and expelled with the steam (as probably occurs in most phreatomagmatic eruptions), juvenile debris, vesiculated to ~50% porosity before erupting, would make up at least 15% the volume of the eruptive deposit. As explained below, the juvenile content of the deposit is probably less than this value.

The evidence for juvenile debris, and the cause of the eruptions at Inyo Craters

The Inyo Craters are among the smallest of the most recent eruptive craters in the Inyo Chain; yet their explosiveness, suggested by eruptive velocities, was comparable to some small maar-type eruptions (Lorenz 1970; Self et al. 1980). The explosiveness of maars and other phreatomagmatic eruptions is generally attributed to the fragmentation of magma and its mixture with groundwater (Sheridan and Wohletz 1983), which increases the surface contact between magma and groundwater and allows heat transfer rates to reach explosive levels. If the eruptions at Inyo Craters were triggered by the heating of groundwater by fragmented magma, one would expect to see a significant percentage of the juvenile debris in the deposits and in the eruptive vent.

Eichelberger et al. (1988) searched the core from the Inyo 4 hole for evidence of juvenile fragments, and found clasts of vesicular rhyolite on the margins of the breccia whose characteristics don't match that of the rhyolitic country rock. Althought the major element

chemistry of this rhyolite is very similar to the rhyolite wall rock, strontium values were nearly twice that of the early rhyolite lava. This evidence, and textures that suggest quenching of clasts, were interpreted by Eichelberger et al. as indications that the vesicular rhyolite may be juvenile. Eichelberger et al. also found some rhyolite clasts in the ejecta with a fresh-appearing, pyroclastic texture. Although these clasts were too small to obtain the strontium concentrations necessary to distinguish these fragments from early rhyolite wall rock, their major element chemistry matched the vesicular rhyolite in the subsurface breccia. Based on this evidence, Eichelberger et al. (1988) hypothesized that the dike fragmented when it encountered groundwater in the gravel layer immediately above the quartzite basement, and that the mixing of magma and groundwater was responsible for the eruptions.

From the lithologic analysis presented in this paper, an attempt was made to estimate the percentage of possibly juvenile debris in the deposit. The estimates of lithology were based on the assumption that point count results of grains 0.25–0.50 mm in diameter represent the lithology of all fragments, 0.06–2.0 mm in diameter; that lapilli count results of fragment 4–7 mm in diameter represent lithologies of fragments 2–64 mm in diameter, and that block count results are representative of the lithology of all larger fragments. The lithology of fragments smaller than 0.06 mm in diameter ($\sim$27% of the deposit) could not be determined quantitatively.

Based on these calculations, approximately 6% of the South Inyo Crater debris of grain diameter lager than 0.06 mm consists of rhyolite glass; almost all of it ash-sized. Two-thirds of this rhyolite glass is non-vesicular and contains elongate plagioclase microlites and/or arcuate perlitic fractures which allow it to be confidently correlated with the perlitic carapace on the early rhyolite flow. The remainder of the glass ($\sim$2%) is either vesicular or lacks microlites, and thus cannot be confidently correlated with the perlitic early rhyolite carapace. Although some fraction of this glass may be juvenile, most of it almost certainly comes from two non-juvenile sources: the early rhyolite tuffs above and below the early rholite flow, and the Inyo tephra which covered the ground surface prior to the eruptions. Thus, if juvenile debris exists in the deposit, it must occur exclusively (or nearly exclusively) in the grain size smaller than 0.25 mm diameter.

This finding led to further discussions with the authors of Eichelberger et al. (1988) regarding the existence or amount of juvenile debris in the deposits. Based on unpublished SEM observations, K. Wohletz and G. Heiken (written communication, 1990) have identified perhaps up to 17% of fragments 0.050–0.250 mm in diameter which are vesicular rhyolite glass, of probable juvenile origin. The inferred origin of these fragments is based on the texture of the vesicles (round as opposed to stretched), and the low abundance of the vesicles relative to vesicular glass fragments from other sources. These fragments are not significantly altered and are therefore probably less than several tens of thousands of years old.

If one assumes that these juvenile fragments compose one fourth of all phreatic debris smaller than 0.25 mm in diameter, they could constitute up to 9% of the total deposit. It seems unlikely that a much larger percentage could exist in the smaller debris without being present in the grain size larger than 0.25 mm diameter. Even with this qualification, the absence in the larger ejecta is truly puzzling. Although grain sizes comparable to those identified by Wohletz at the Inyo Craters are not uncommon for silicic phreatomagmatic ejecta (Self and Sparks 1978; Wohletz 1986; Sheridan and Wohletz 1983; Heiken et al. 1986), most such grain-size measurements have been made on airfall or surge deposits where a certain amount of sorting took place. The percentage and grain size of fine juvenile glass in deposits that otherwise appear to consist only of accidental debris is, as far as this author knows, almost totally unstudied. Whether the volume of juvenile debris apparently hidden in the Inyo Craters deposits could have driven the Inyo Craters eruptions is not clear, although the energy calculations presented earlier seem to suggest that it was unlikely.

An alternative possibility is that groundwater was heated rapidly by fragmenting magma, but that the steam was physically separated from the magma fragments, leaving them behind in the vent before it erupted. How such a separation could take place is a matter of speculation, but one possibility is that, following fragmentation, steam rose upward through fractures without sufficient speed to entrain the larger magma particles, and the eruption shut off before much juvenile debris reached the surface.

A second possibility is that most heat transfer to groundwater took place without fragmentation. Such heating would have to have occurred over a long period of time. Delaney (1982) has argued that the heating of groundwater in the wall rock near a rapidly emplaced dike causes a steam layer to form near the dike wall, after which heat flow occurs at roughly conductive rates until convection cells become established. For typical rock thermal diffusivities, a dike of a thickness of 2 to 90 m would have dissipated half of its heat in a time ranging from several weeks to several decades (Delaney 1987). The water must have been held in a relatively porous and probably permeable unit (perhaps the till immediately above the basement) that would have allowed water to escape rapidly during the eruption. Yet in order to allow pressure to build up and to prevent the heated water from slowly escaping, this unit would have to have been confined by low-permeability surrounding units. Additionally, the eruption would have to have been triggered not by heating (because heating was not rapid enough), but by a second event; perhaps pressure buildup, subsequent intrusive activity, or tectonic deformation that would have breached the confinement. As pointed out by J. C. Eichelberger (Sandia National Laboratories, 1990) in a review of this paper, the surface area over which heat could be transferred would be a few to several times greater, and the time required to heat a sufficient amount of groundwater correspondingly less, if water were heated along

the sides of the dike in the uppermost few hundred meters of basement below the base of the till. Basement rocks are highly fractured in drill core and could perhaps have contained a significant amount of water.

A third possibility is that a dike intrusion breached the confinement of a pre-existing geothermal aquifer in the Bishop Tuff. This hypothesis is simpler than the last in the sense that slow heating of groundwater prior to the eruption would not have to be invoked. On the other hand, there is no direct evidence (in the form of Bishop Tuff fragments in the deposits) that flow originated in the Bishop Tuff. Additionally, the Bishop Tuff may not directly underlie the Inyo Craters, and flow of hot water would have had to follow a longer and perhaps more circuitous route than that from the gravel above the basement. The drilling data available are clearly not sufficient to resolve the complexities of such a route.

Concluding remarks

The evidence presented by Eichelberger et al. (1988) suggests that magma was directly involved in the eruptions of the Inyo Craters. However the lack of a large amount of juvenile debris in the deposit, the confinement of juvenile fragments to the smallest grain-size fractions, and the energy considerations presented in this paper make it questionable whether the heat in the juvenile debris actually powered the eruption, or whether they were incidental fragments in an eruption which was powered by other mechanisms. The "other" mechanisms suggested in this paper are necessarily more complicated than the fragmentation mechanism, because they require slow heating, storage, and the sudden release of hot, pressurized water, or the existence of an older geothermal system, rather than simply rapid heating and expulsion. In addition, they require a longer time and probably a somewhat complicated hydrologic system, and are not easy to conceptualize, especially in regions where subsurface structure and the timing of intrusive events are poorly known. The availability of subsurface information at Inyo Craters has helped significantly in constraining the number of possible eruption mechanisms, but considerably more work is needed to identify specifically how this eruption (and phreatic eruptions in general) occurred. It is hoped that future research will help solve these important and difficult problems.

Appendix: Ballistic analysis

The eruption velocities at Inyo Craters were modelled using a set of analytical equations for the flight of ballistic blocks derived by Minakami (1942). The differential equations that govern the block trajectories during flight are:

$$m\frac{du_x}{dt} = -F_x$$

$$m\frac{du_z}{dt} = -\mathrm{mg} - F_z$$

where m is the mass of the block (which depends on the block density, ρ_r, and its radius, r), u_x and u_z are the horizontal and vertical velocity components, respectively, t is time, g is the gravitational constant, and F_x and F_z are the horizontal and vertical components of the drag force acting on the block due to air friction. For Newton's drag law (where the drag force is proportional to the velocity squared), $F_z \propto u_z^2 \csc\theta$, and $F_x \propto u_x^2 \sec\theta$. Because the differential equations are coupled via the trajectory angle, θ, they cannot be solved analytically (Sherwood 1967). They can be uncoupled, however, by dropping the θ terms in each equation and by assuming that $F_z \propto u_z^2$, and $F_x \propto u_x^2$. This amounts to underestimating the total drag force along the trajectory by the factor $(\sin^4\theta + \cos^4\theta)^{1/2}$ (Sherwood 1967). The drag forces are related to the drag coefficient, C_D, by the expressions (Bird et al. 1960, p. 182):

$$F_x = \frac{1}{2}\rho_a C_D A u_x^2$$

$$F_z = \frac{1}{2}\rho_a C_D A u_z^2$$

where ρ_a is the air density, and A is the cross sectional area of the block. Substituting these expressions into the previous equations, and replacing u_x and u_z with the derivatives of x and z with respect to t, we obtain:

$$m\frac{d^2z}{dt^2} = -mg - \frac{1}{2}\rho_a C_D A\left(\frac{dz}{dt}\right)^2$$

for a rising block, and:

$$m\frac{d^2z}{dt^2} = -mg + \frac{1}{2}\rho_a C_D A\left(\frac{dz}{dt}\right)^2$$

for a falling block, in the vertical plane. In the horizontal plane, incorporating a term (W) for the speed of a horizontal wind blowing away from the source,

$$m\frac{d^2u_x}{dt^2} = \frac{1}{2}\rho_a C_D A\left(\frac{dx}{dt} - W\right)^2$$

Integration of these equations gives the following analytical solutions for the range (X_m) and time of flight (t_T) of the block.

$$X_m = \frac{1}{\mu}\ln(\mu(u_o\cos\theta - W)t_T + 1) + Wt_T$$

$$t_T = \frac{1}{\sqrt{\mu g}}\left(\cosh^{-1}\left(\sqrt{1+\frac{\mu}{g}u_o^2\sin^2\theta}\right) + \tan^{-1}\sqrt{\frac{\mu}{g}}u_o\sin\theta\right)$$

where u_o is the initial velocity, nd θ is the initial trajectory angle from horizontal. The term μ is defined as

$$\mu = \frac{1}{2}\rho_a\frac{C_D A}{m}$$

Correcting for the altitude difference, ξ, of the crater floor above the point of deposition, t_T becomes:

$$t_T = \frac{1}{\sqrt{\mu g}} \left(\cosh^{-1} \left(\sqrt{1 + \frac{\mu}{g} u_o^2 \sin^2\theta} \cdot \exp(\xi\mu) \right) + \tan^{-1} \sqrt{\frac{\mu}{g}} u_o \sin\theta \right)$$

Except for high trajectory angles ($\theta > \sim 70°$), these equations give results that are within 20% of those of more accurate, numerical solutions that do not ignore the coupling of the θ terms in the differential equations (Sherwood 1967).

Values of C_D used in past studies have varied from 0.44 to 1.0 (Self et al. 1980). The choice of 1.0 used in this study is based on the irregular shapes of the blocks, which would give them relatively high C_D values. The density of air at 25° C at ambient pressure at 2500 m elevation is 0.884 kg/m^3, but the air density (ρ_a) appropriate for these equations could vary from approximately 0.590 kg/m^3 (the density of steam at 100° C and ambient pressure) to a few times 0.884 kg/m^3 depending on the pressure of the steam blast. Variations in the value of C_D between 0.6 and 1.0, and variations in ρ_a up to 35% change X_m by less than 10%.

A trajectory angle (θ) of 45° was used in these calculations because, according to the equations of Minakami, it gives the greatest range for a particular velocity. Steinberg (1977) notes that maximum ranges are obtained for $\theta = 63$–$65°$; however his calculations assume an increase in ejection velocity with increasing ejection angle. By assuming $\theta = 45°$, one obtains a conservative estimate of the maximum velocity for a given range.

Acknowledgements. This research was supported by the Department of Energy, Office of Basic Energy Sciences, under grant DE-FG03-85ER13319. The drilling team from Sandia Laboratories was especially helpful in providing drilling information. Discussions with John Eichelberger helped form many of my thoughts on the origin of the craters and the nature of the eruption. Careful, critical reviews of this manuscript by my former advisor at Stanford University, David Pollard, graduate committee members Gail Mahood and Roy Bailey, and by Ken Wohletz and Grant Heiken, have helped this paper considerably.

References

Bailey RA (1989) Geologic map of the Long Valley Caldera, Mono-Inyo Craters Volcanic Chain, and Vicinity, eastern California. US Geol Surv Misc Invest Map I-1933

Bailey RA, Dalrymple GB, Lanphere MA (1976) Volcanism, structure, and geochronology of Long Valley Caldera, Mono County, California. J Geophys Res 81:725–744

Bailey RA, MacDonald RA, Thomas JE (1983) The Inyo-Mono Craters: products of an actively differentiating rhyolite magma chamber, eastern California. Eos 64:336

Bird RB, Stewart WE, Lightfoot EN (1960) Transport phenomena. John Wiley and Sons, New York, pp 1–780

Christiansen RL, Peterson DW (1981) Chronology of the 1980 eruptive activity. In: The 1980 eruptions of Mt St Helens, Washington. US Geol Surv Prof Paper 1250

Delaney PT (1982) Rapid intrusion of magma into wet rock: groundwater flow due to pore pressure increases. J Geophys Res 87:7739–7756

Delaney PT (1987) Heat transfer during emplacement and cooling of mafic dykes. In: Geol Assoc Canada Spec Paper on Mafic Dyke Swarms, pp 31–46

Eichelberger JC, Vogel TA, Younker LW, Miller CD, Heiken GH, Wohletz KH (1988) Structure and stratigraphy beneath a young phreatic vent: South Inyo Crater, Long Valley Caldera, California. J Geophys Res 93:13 208–13 220

Feuillard M, Allegre CJ, Brandeis G, Gaulon R, Le Mouel JL, Mercier JC, Pozzi JC, Semet MP (1983) The 1975–1977 crisis of La Soufriere de Guadeloupe (F.W.I.): a still-born magmatic eruption. J Volcanol Geotherm Res 16:317–334

Fink JH (1985) The geometry of silicic dikes beneath the Inyo domes, California. J Geophys Res 90:11 127–11 133

Finch RH (1943) Lava surgings in Halemaumau and the explosive eruptions in 1924. Volcano Lett 479:1–4

Fisher RV (1968) Puu Hou littoral cones, Hawaii. Geol Rundsch 57:837–864

Fisher RV, Schmincke H-U (1984) Pyroclastic rocks. Springer, Berlin Heidelberg New York, pp 1–472

Fudali RF, Melson WG (1972) Ejecta velocities, magma chamber pressure and kinetic energy associated with the 1968 eruption of Arenal volcano. Bull Volcanol 35:383–401

Hedenquist JW, Henley RW (1985) Hydrothermal eruptions in the Waiotapu Geothermal System, New Zealand: their origin, associated breccias, and relation to precious metal mineralization. Econ Geol 80:1640–1668

Gorshkov GS (1959) Gigantic eruption of the Bezymianny volcano. Bull Volcanol 2:20

Heiken GH, Goff F, Stix J, Tamanyu S, Shafiqullah M, Garcia S, Hagan R (1986) Intracaldera volcanic activity, Toledo Caldera and Embayment, Jemez Mountains, New Mexico. J Geophys Res 91:1799–1815

Huber NK, Rinehart CD (1965) Geologic map of the Devil's Postpile quadrangle, Sierra Nevada, California. US Geol Surv Map GQ-437

Le Guern F, Bernard A, Chevrier RM (1980) Soufriere of Guadeloupe 1976–77 eruption-mass and energy transfer and volcanic health hazards. Bull Volcanol 43-3:577–593

Lloyd EF (1959) The hot springs and hydrothermal eruptions of Waiotapu. New Zealand J Geol Geophys 2:141–176

Lorenz V (1970) Some aspects of the eruption mechanism of the Big Hole Maar, central Oregon. Bull Geol Soc Am 81:1823–1830

Lorenz V (1973) On the formation of maars. Bull Volcanol 37:183–204

Lorenz V (1986) On the growth of maars and diatremes and its relevance to the formation of tuff rings. Bull Volcanol 48:265–274

Mastin LG, Pollard DD (1988) Surface deformation and shallow dike intrusion processes at Inyo Craters, Long Valley, CA. J Geophys Res 93:13 221–13 235

Metz JM, Mahood GA (1985) Precursors to the Bishop Tuff eruption: Glass Mountain, Long Valley, California. J Geophys Res 90:11 121–11 126

Miller CD (1985) Holocene eruptions at the Inyo Volcanic Chain, California – Implications for possible eruptions in Long Valley Caldera, Geology 13:14–17

Minakami T (1942) On the distribution of volcanic ejecta (part I). The distributions of volcanic bombs ejected by the recent explosions of Asama. Bull Earthquake Res Inst Tokyo 20:65–91

Moore JG, Nakamura K, Alcaraz A (1966) The 1965 eruption of Taal Volcano, Science 151:955–960

Muffler LJP, White DE, Truesdell AH (1971) Hydrothermal explosion craters in Yellowstone National Park. Geol Soc Am Bull 82:723–740

Nairn IA (1979) Rotomahana-Waimangu eruption, 1886: base surge and basalt magma. New Zealand J Geol Geophys 22:363–378

Nairn IA, Wiradiradja S (1980) Lae Quaternary hydrothermal explosion breccias at Kawerau Geothermal Field, New Zealand. Bull Volcanol 43:1–13

Nairn IA, Wood CP, Hewson CAY (1979) Phreatic eruptions of Ruapehu: April 1975. N Zealand J Geol Geophys 22:155-173

Nakamura K (1964) Volcano-stratigraphic study of Oshima Volcano Izu. Bull Earthquake Res Inst, Tokyo 42:649-728

Nelson CE, Giles DL (1985) Hydrothermal eruption mechanisms and hot spring gold deposits. Econ Geol 80:1633-1639

Pollard DD, Fink JH, Delaney PT (1984) Igneous dikes at Long Valley, CA: emplacement mechanisms and associated geologic structures, US Geol Surv Open File Rep 84-939:130-146

Prinz M (1970) Idaho rift system, Snake River Plain, Idaho. Bull Geol Soc Am 81:941-948

Sampson DE, Cameron KL (1987) The geochemistry of the Inyo Volcanic Chain: Multiple magma systems in the Long Valley region, eastern California. J Geophys Res 92:10403-10421

Self S, Sparks RSJ (1978) Characteristics of wide-spread pyroclastic deposits formed by the interaction of silicic magma and water. Bull Volcanol 41:196-212

Self S, Kienle J, Huot JP (1980) Ukinrek maars, Alaska, II. Deposits and formation of the 1977 craters. J Volcanol Geotherm Res 7:39-65

Shepherd JB, Sigurdsson H (1982) Mechanism of the 1979 explosive eruption of Soufriere volcano, St. Vincent. J Volcanol Geotherm Res 13:119-130

Sheridan MF, Wohletz KH (1983) Hydrovolcanism: Basis considerations and review. J Volcanol Geotherm Res 17:1-29

Sherwood AE (1967) Effect of air drag on particles ejected during explosive cratering. J Geophys Res 72:1783-1791

Sieh K, Bursik M (1986) Most recent eruption of the Mono Craters, eastern central California. J Geophys Res 91:12539-13571

Sorey ML (1985) Evolution and present state of the hydrothermal system in Long Valley Caldera. J Geophys Res 90:11219-11228

Sorey ML, Suemnicht GA, Sturchio NC, Nordquist GA (1991) New evidence on the hydrothermal system in Long Valley Caldera, California from wells, fluid sampling, electrical geophysics, and age determinations of hot-spring deposits. J Volc Geotherm Res. in press

Steinberg GS (1977) On the determination of the energy and depth of volcanic explosions. Bull Volcanol 40:116-120

Suemnicht GA (1987) Results of deep drilling in the western moat of Long Valley, California. Eos 68:785-798

Suemnicht GA, Varga RJ (1988) Basement structure and implications for hydrothermal circulation patterns in the western moat of Long Valley Caldera, California. J Geophys Res 93:13191-13207

Walker GPL (1971) Grain-size characteristics of pyroclastic deposits. J Geol 79:696-714

White DE (1955) Violent mud-volcano eruptions of Lake City Hot Springs, northeastern California. Bull Geol Soc Am 66:1109-1130

Whyte F (1968) Lower Carboniferous volcanic vents in the west of Scotland. Bull Volcanol 32:253-268

Williams H, McBirney AR (1979) Volcanology. Freeman, San Francisco, pp 1-391

Wilson L, Head JW III (1981) Ascent and eruption of basaltic magma on the Earth and moon. J Geophys Res 86:2971-3001

Wohletz KH (1986) Explosive magma-water interactions: thermodynamics, explosion mechanisms, and field studies. Bull Volcanol 48:245-264

Wohletz KH, McQueen RG (1984) Experimental studies of hydromagmatic volcanism. In: Explosive volcanism: inception, evolution, and hazards. National Academy Press, Washington, pp 158-169

Wohletz KH, Sheridan MF (1983) Hydrovolcanic explosions II. Evolution of basaltic tuff rings and tuff cones. Am J Sci 283:385-413

Wood S (1977) Distribution, correlation, and radiometric dating of late Holocene tephra, Mono and Inyo Craters, eastern California. Geol Soc Am Bull 88:89-95

Yokoyama I (1956) Energetics in active volcanoes. 1st paper. (Activities of volcano Mihara, Ooshima Island during the period 1953-54). Tokyo Univ Bull Earthquake Res Inst 34:190-195

Yokoyama I Energetics in active volcanoes. 2nd paper. Tokyo Univ Bull Earthquake Res Inst 35:75-97

Editorial responsibility: H.-U. Schmincke